CHAPTER

S10

Pacific Ocean: Supplementary Materials

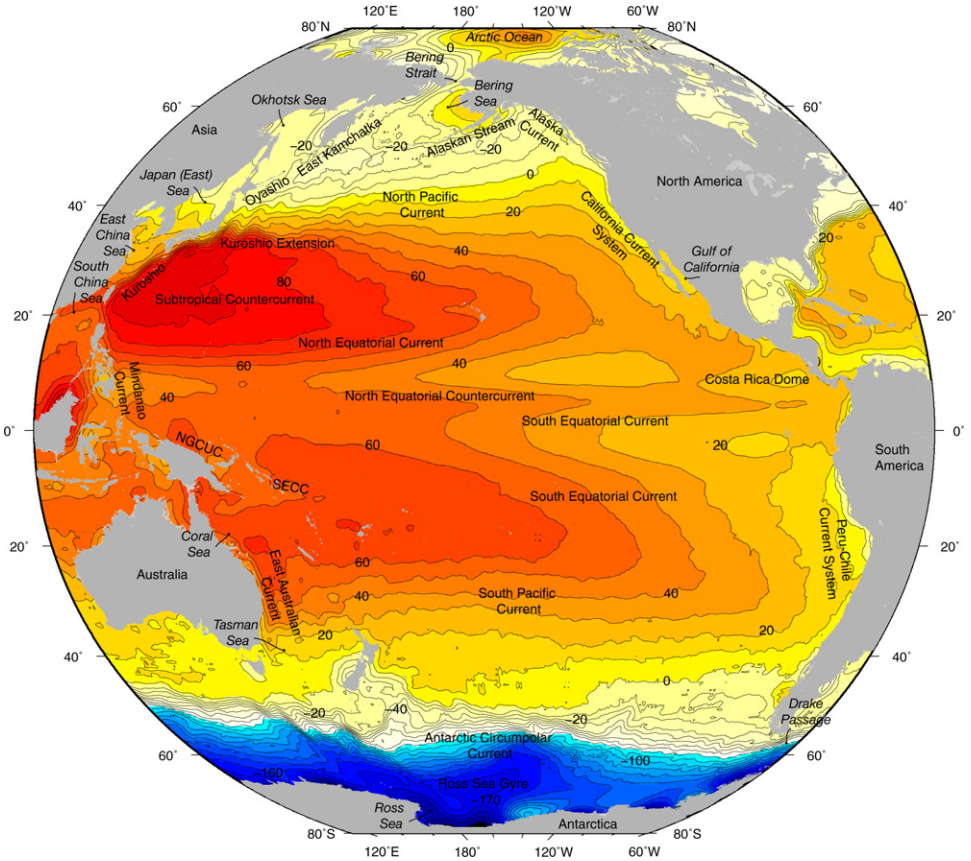

FIGURE S10.1 Pacific Ocean: mean surface geostrophic circulation with the current systems described in this text. Mean surface height (cm) relative to a zero global mean height, based on surface drifters, satellite altimetry, and hydrographic data. (NGCUC = New Guinea Coastal Undercurrent and SECC = South Equatorial Countercurrent). *Data from Niiler, Maximenko, and McWilliams (2003).*

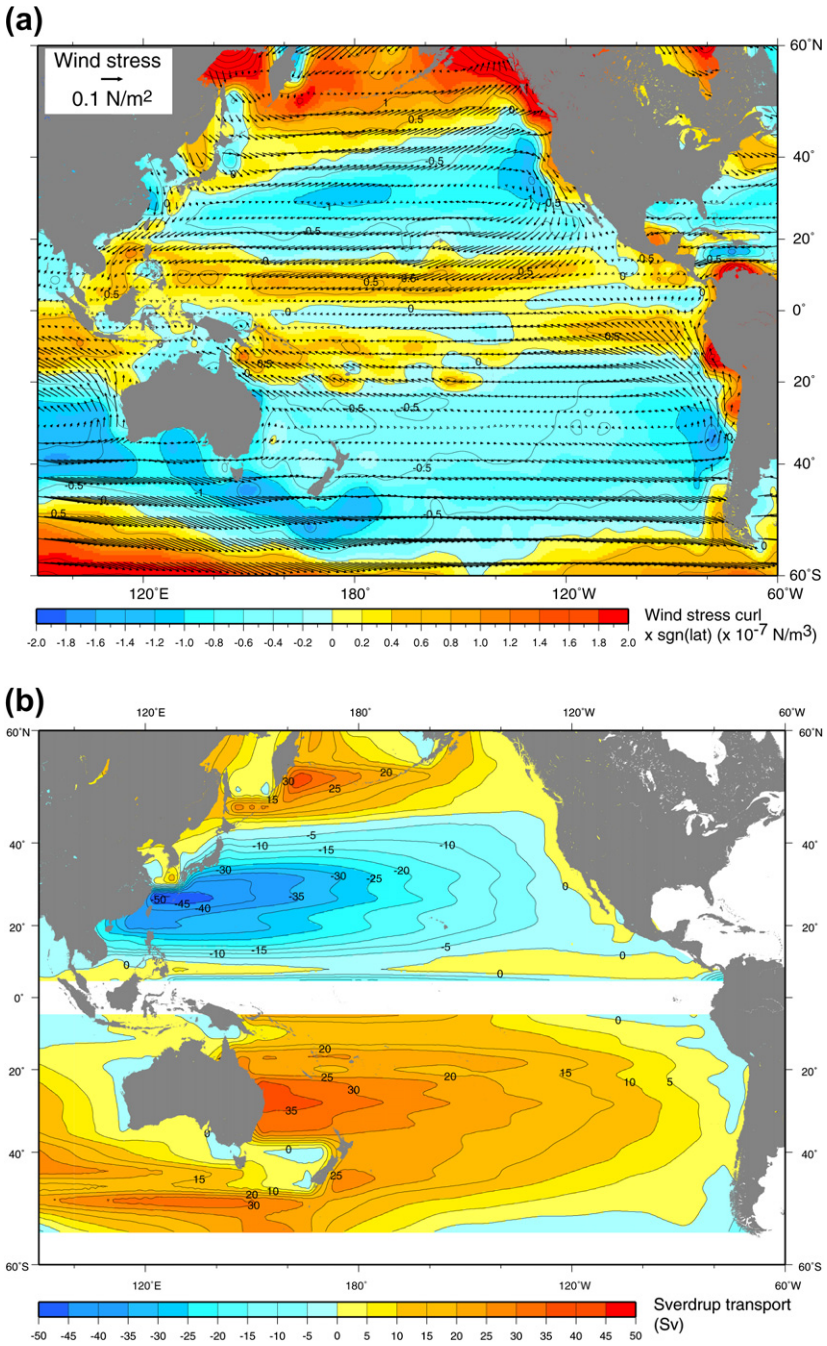

FIGURE S10.2 Annual mean winds. (a) Wind stress (N/m^2) (vectors) and wind-stress curl ($\times 10^{-7}$ N/m^3) (color), multiplied by -1 in the Southern Hemisphere. (b) Sverdrup transport (Sv), where blue is clockwise and yellow-red is counterclockwise circulation. *Data from NCEP reanalysis (Kalnay et al.,1996).*

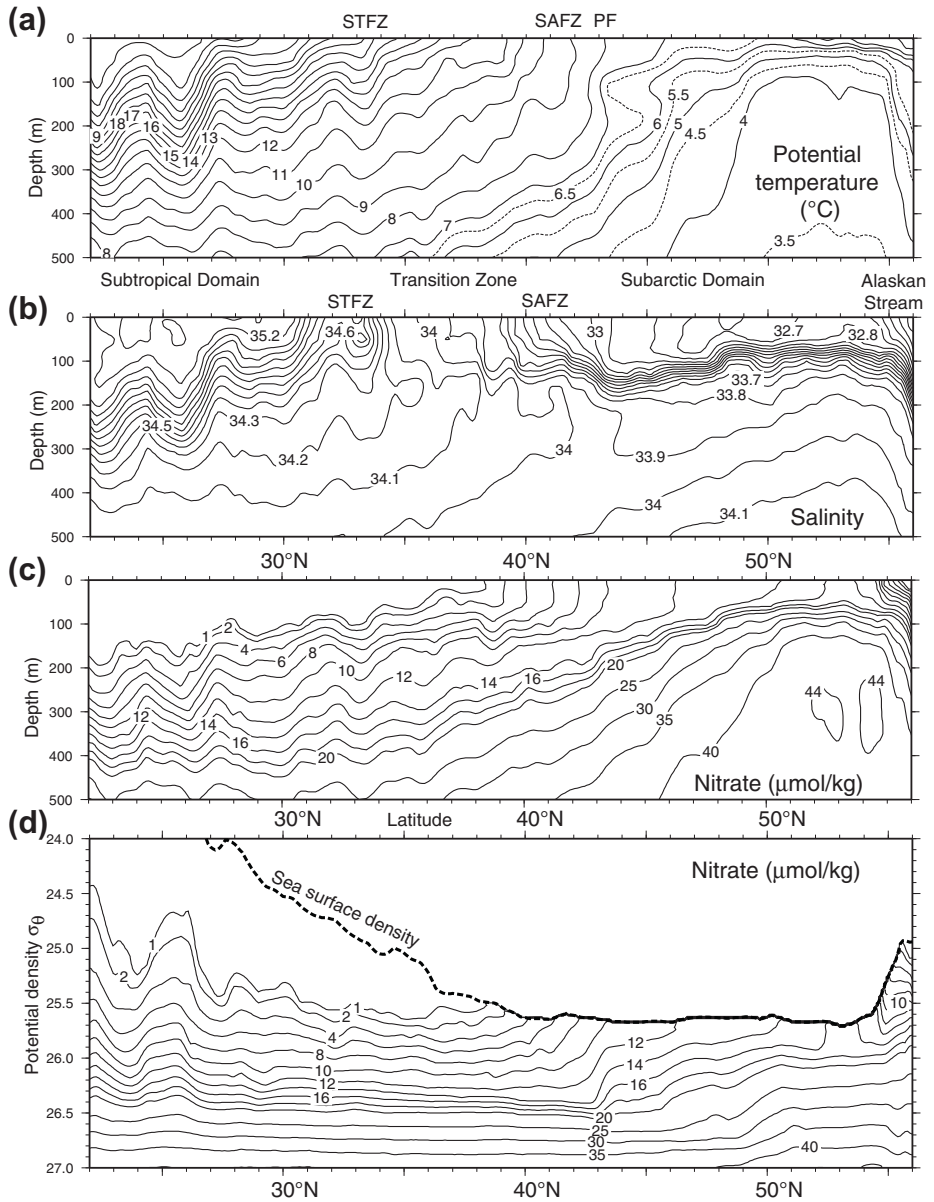

FIGURE S10.3 The subtropical-subarctic transition along 150°W in the central North Pacific (May–June, 1984). SAFZ and STFZ: subarctic and subtropical frontal zones. (a) Potential temperature (°C), (b) salinity, (c) nitrate (µmol/kg), and (d) nitrate versus potential density. *After Roden (1991).* Data from WOCE Pacific Ocean Atlas; Talley (2007).

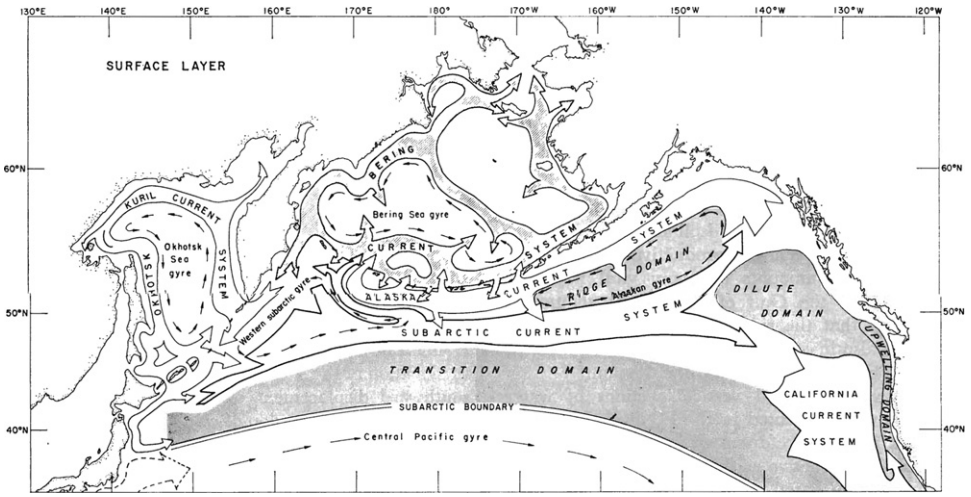

FIGURE S10.4 Subpolar gyre regimes. Only the major features are described in the text. *Source: From Favorite, Dodimead, and Nasu (1976).*

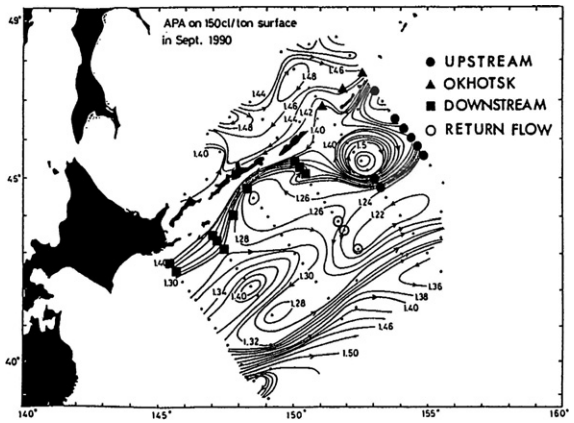

FIGURE S10.5 Oyashio. Acceleration potential anomaly (similar to geopotential anomaly) on the isopycnal $\sigma_\theta = 26.52$ kg/m^3 (150 cl/ton) referenced to 1500 dbar in September 1990. *Source: From Kono and Kawasaki (1997).*

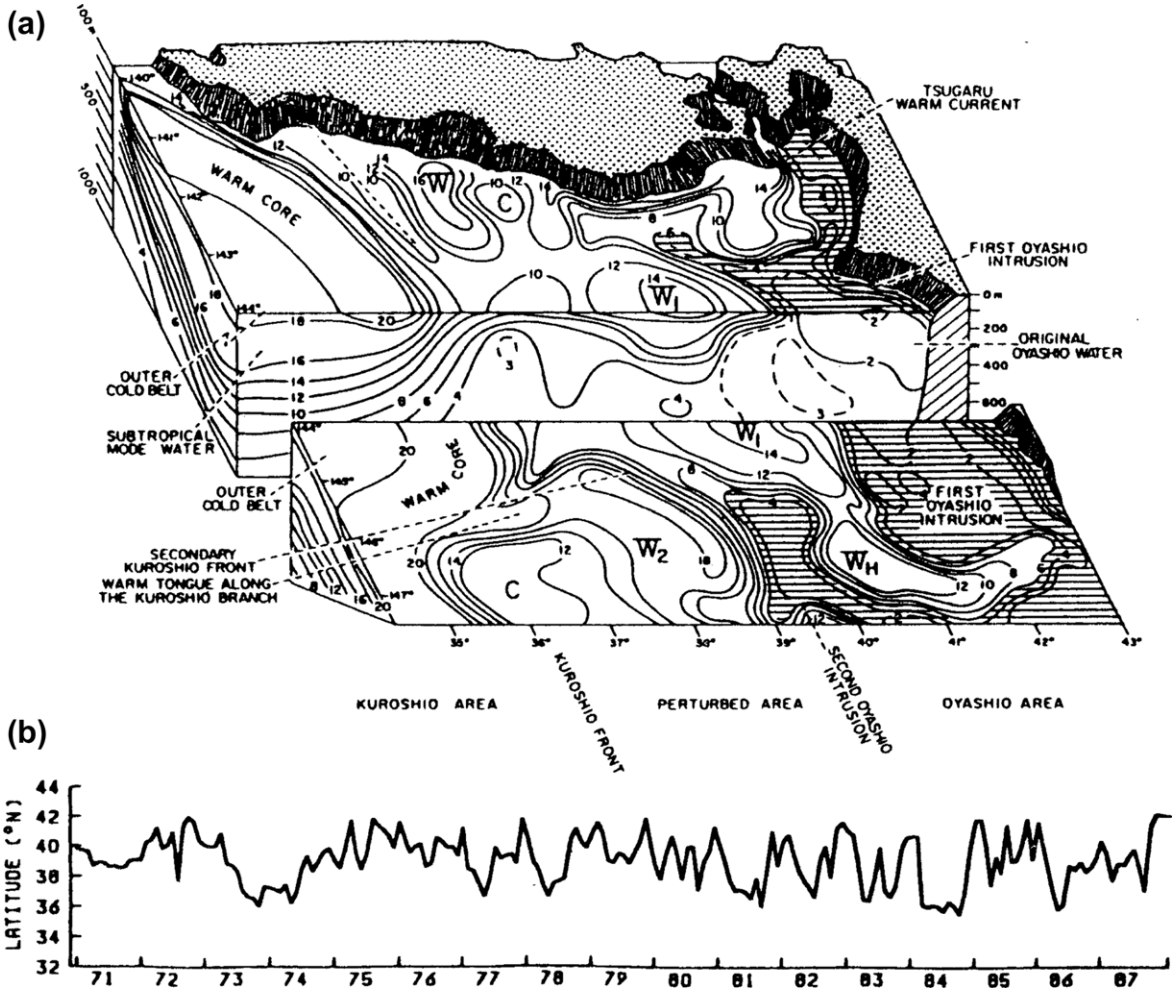

FIGURE S10.6 (a) The Oyashio, Kuroshio, and Mixed Water Region east of Japan. (b) The southernmost latitude of the first Oyashio intrusion east of Honshu. *Source: From Sekine (1999).*

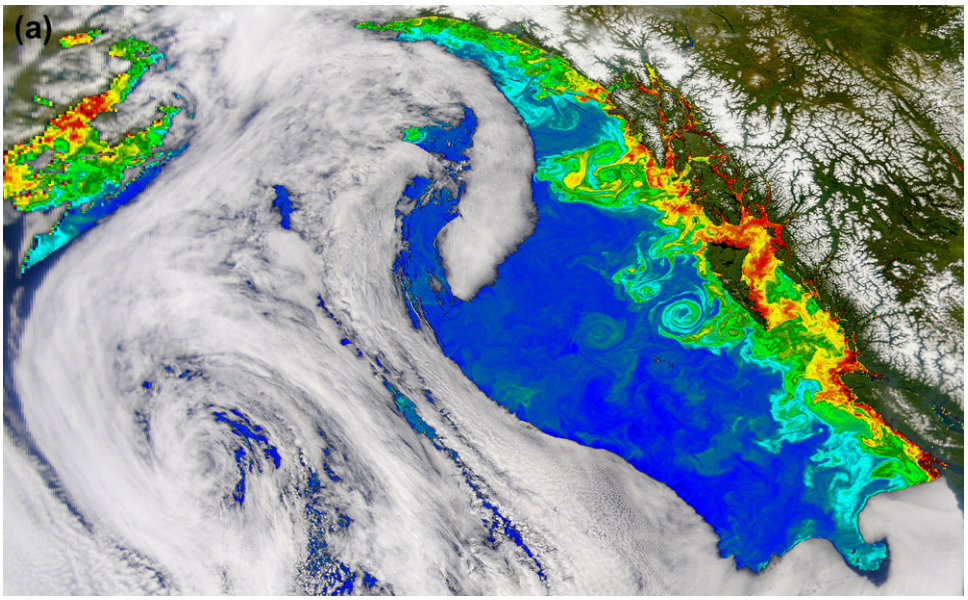

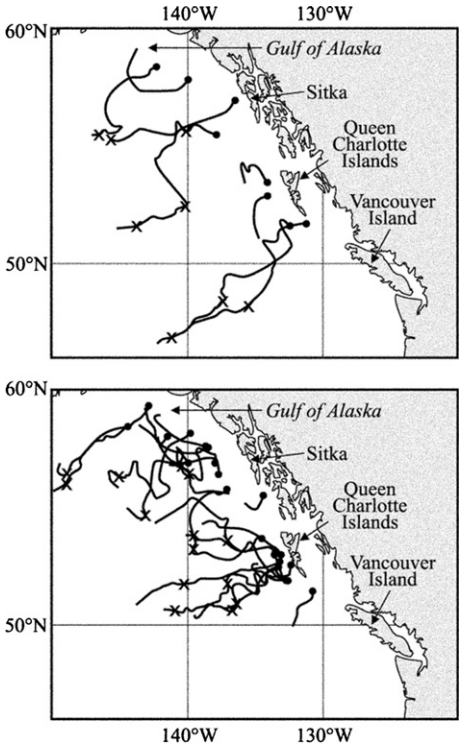

FIGURE S10.7 (a) Ocean color from the SeaWIFS satellite, showing an anticyclonic Haida Eddy in the Alaska Current on June 13, 2002. *Source: From NASA Visible Earth (2008)*. (b) Tracks of Sitka and Haida Eddies in 1995 and 1998 (top right) and in remaining years between 1993 and 2001 (bottom right). *Source: From Crawford (2002).*

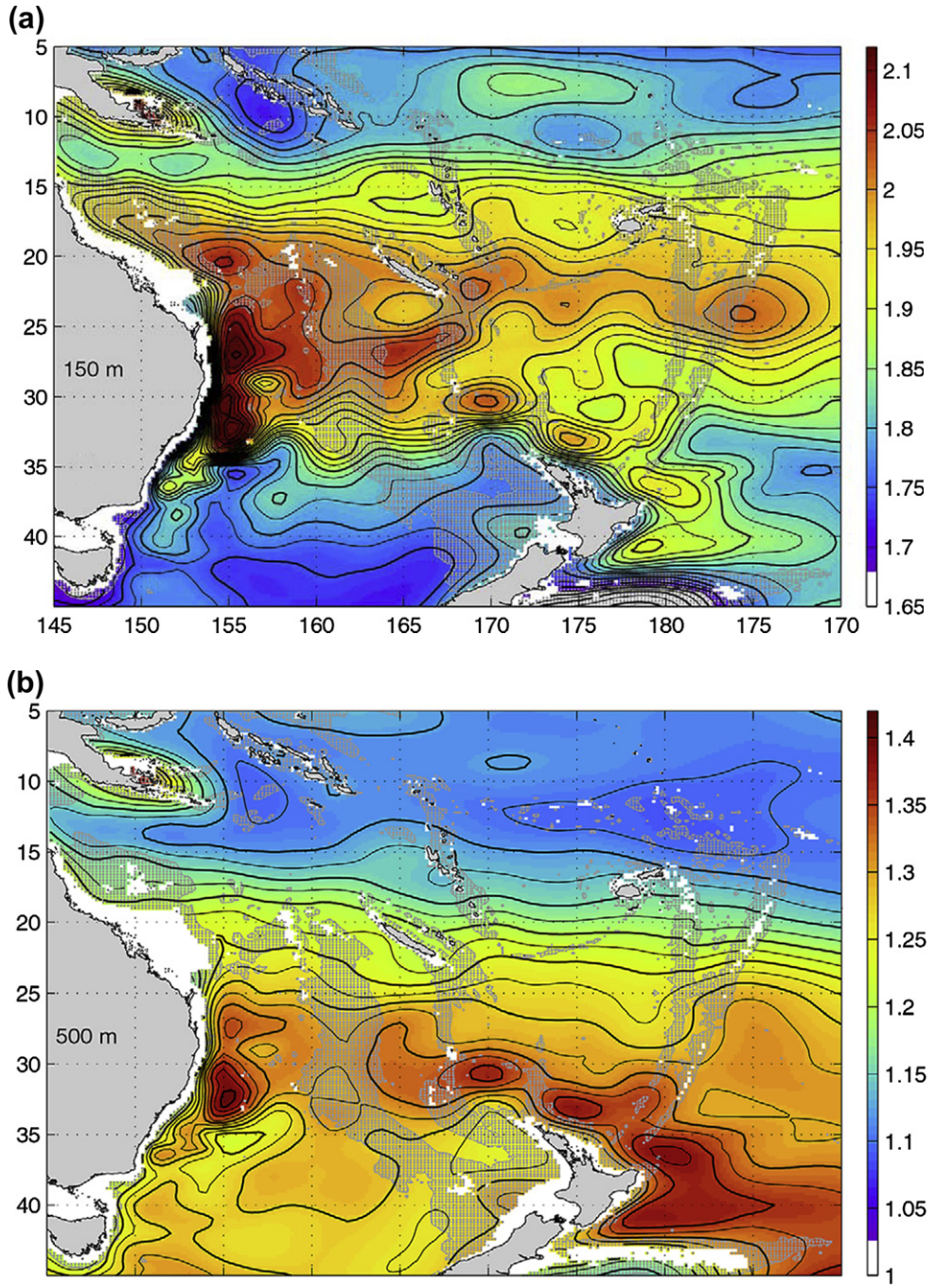

FIGURE S10.8 Mean steric height at (a) 150 m and (b) 500 m relative to 2000 m; contour intervals are 0.04 and 0.02 m, respectively. *Source: From Ridgway and Dunn (2003).*

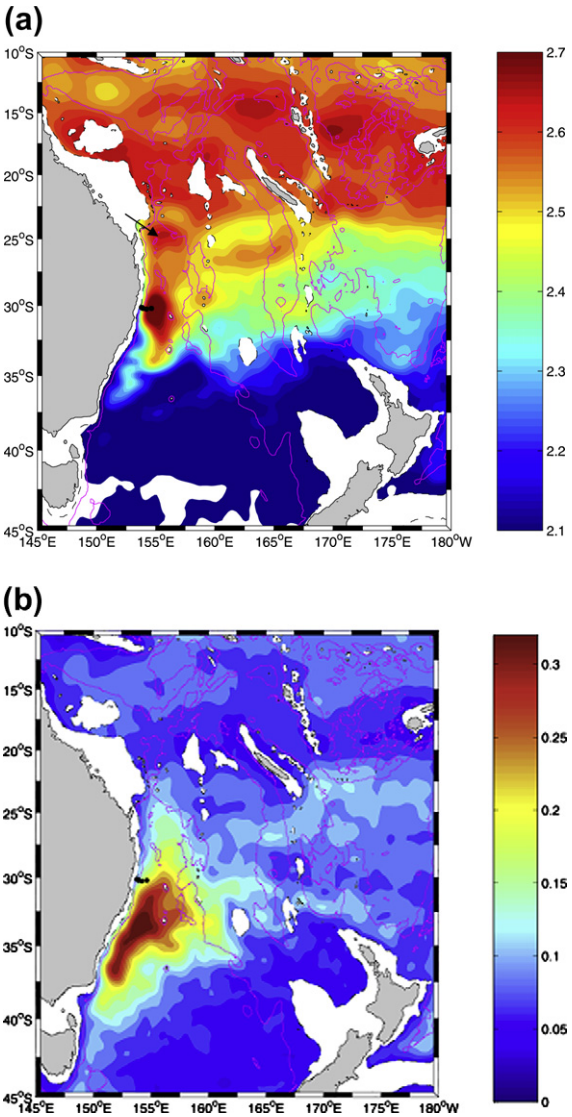

FIGURE S10.9 Sea level (m). (a) Total sea level, and (b) RMS sea level anomalies, from satellite altimetry. The 3000 m isobath is shown (purple). *Source: From Mata, Wijffels, Church, and Tomczak (2006).*

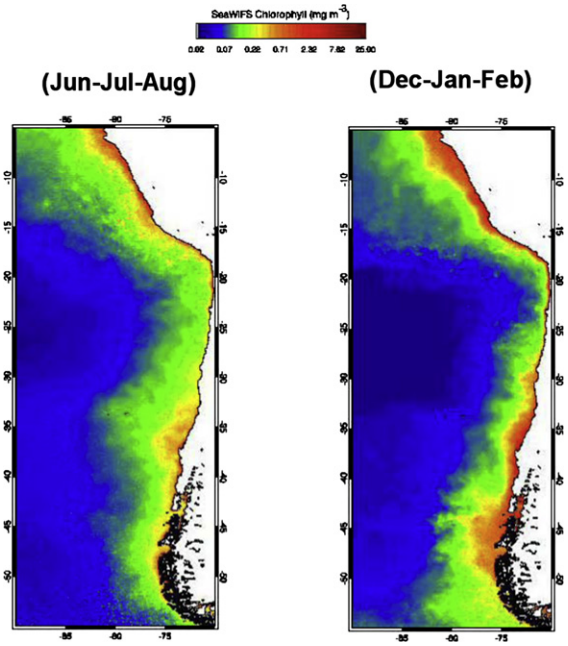

FIGURE S10.10 Surface chlorophyll concentration in austral winter (June, July, August) and summer (December, January, February), derived from SeaWiFS satellite observations. *Source: From Mackas, Strub, Thomas, and Montecino (2006).*

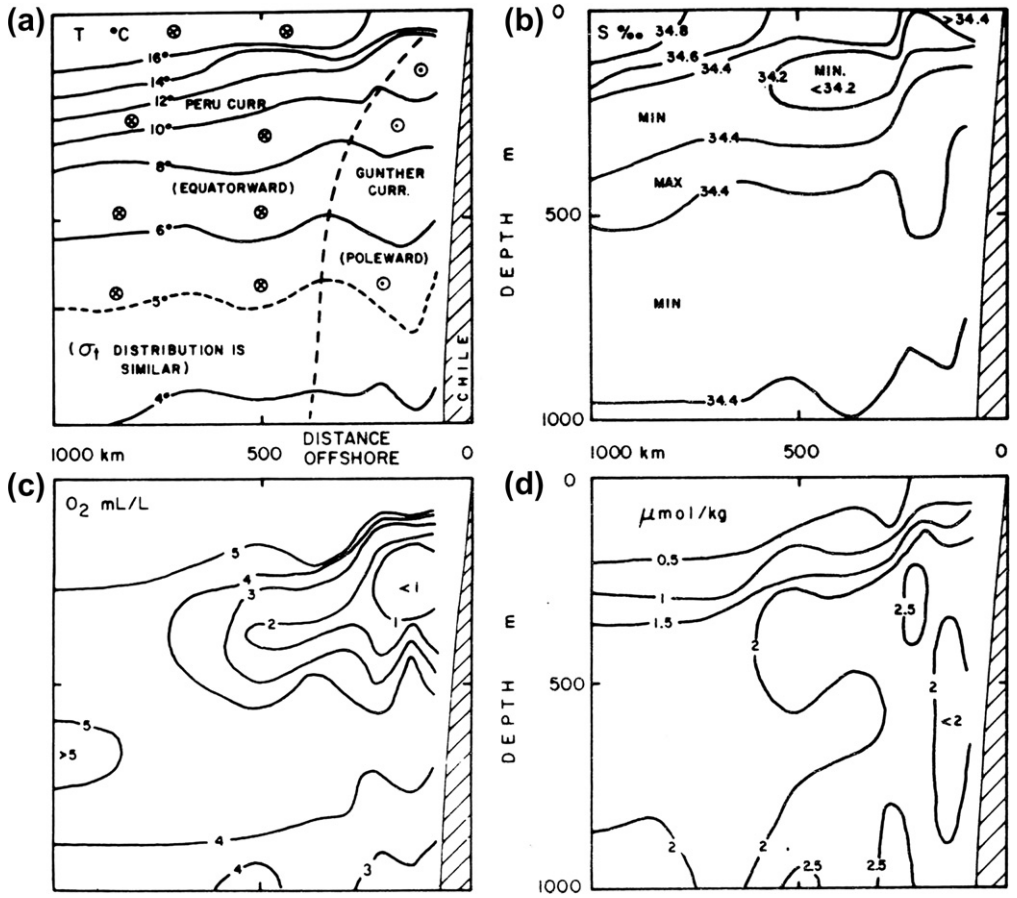

FIGURE S10.11 Eastern South Pacific zonal vertical sections at 33°S: (a) temperature with meridional current directions, (b) salinity, (c) dissolved oxygen, and (d) phosphate.

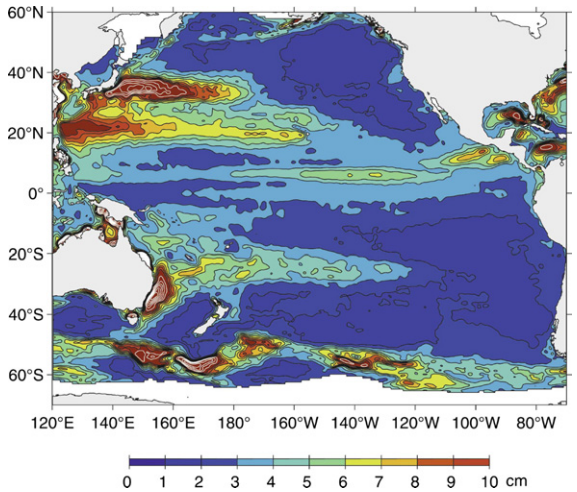

FIGURE S10.12 RMS variability in surface height (cm) from satellite altimetry, high-passed with half power at 180 days to depict the mesoscale eddy energy. ©American Meteorological Society. Reprinted with permission. *Source: From Qiu, Scott, and Chen (2008).*

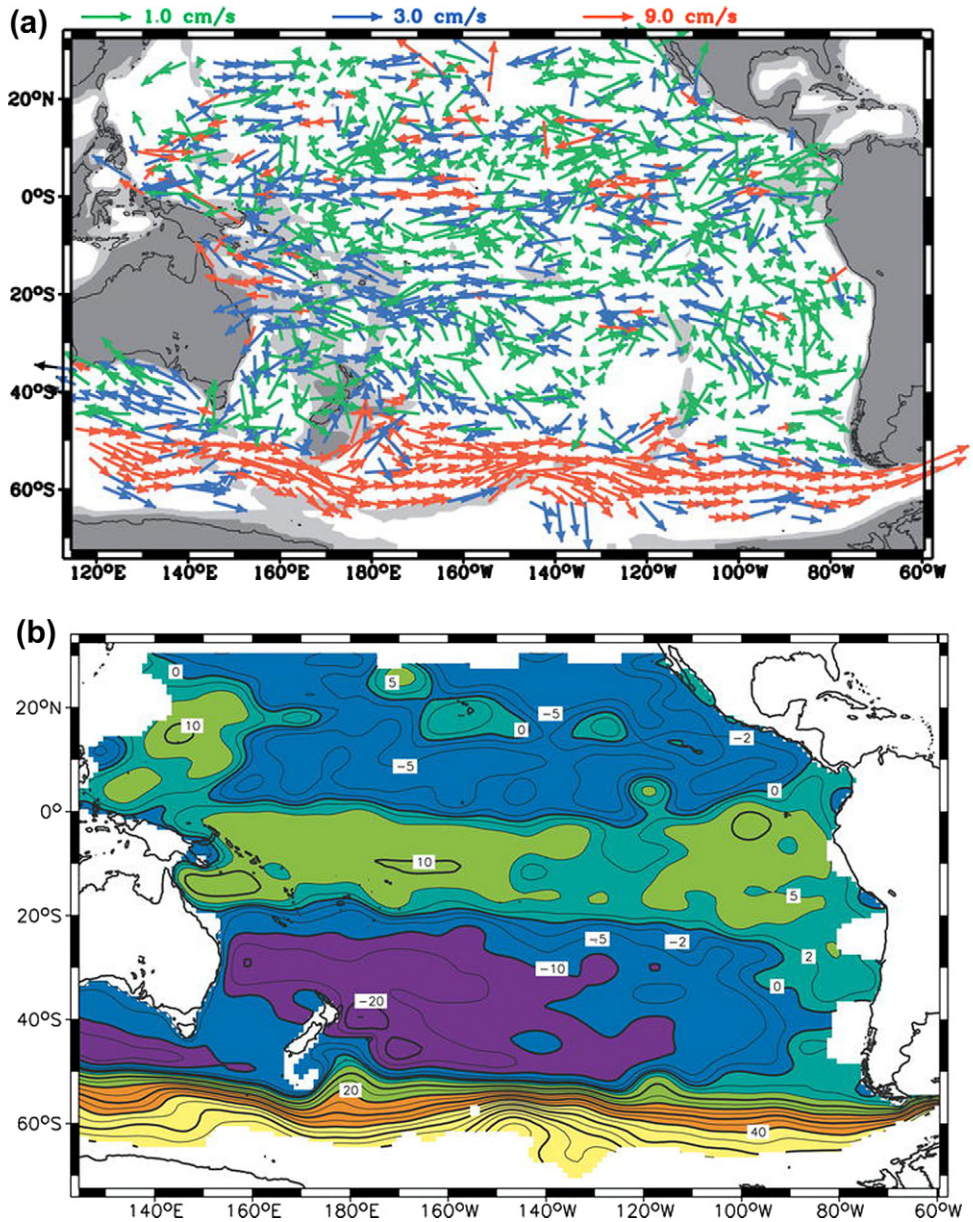

FIGURE S10.13 Mean flow at 900 m depth in the tropical and South Pacific based on subsurface float observations. (a) Velocity (cm/sec). (b) Geostrophic streamfunction (1000 m^2/s). ©American Meteorological Society. Reprinted with permission. *Source: From Davis (2005).*

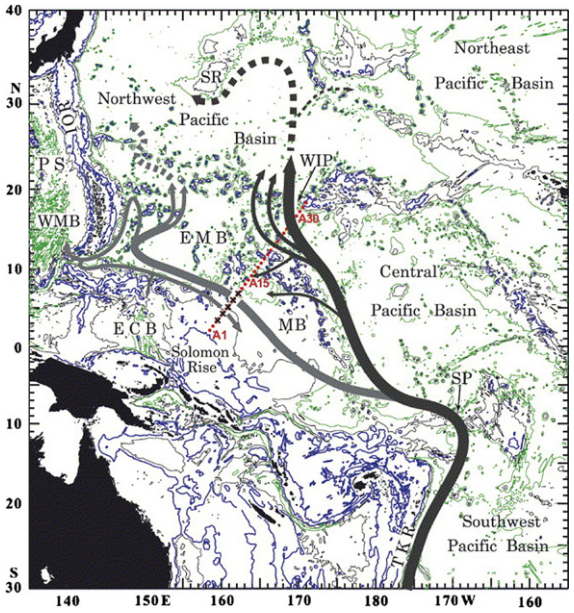

FIGURE S10.14 Pacific abyssal circulation schematics. Low latitude North Pacific. *Source: From Kawabe, Yanagimoto, and Kitagawa (2006).*

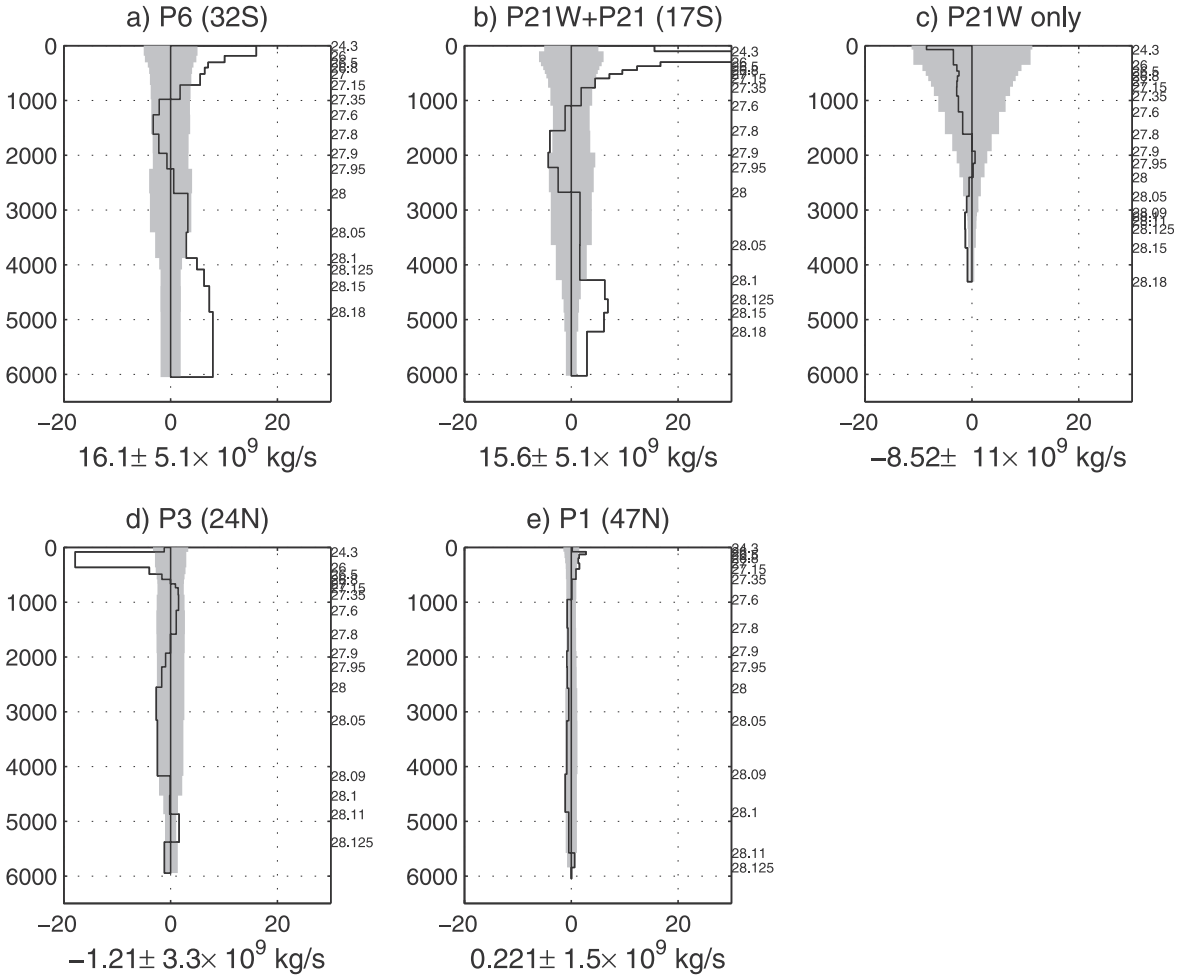

FIGURE S10.15 Northward transports (Sv) across zonal sections in isopycnal layers, integrated upwards from zero at the bottom. Section latitudes are indicated in parentheses. Ekman transport is not included. Gray indicates the uncertainty. *Source: From Ganachaud (2003).*

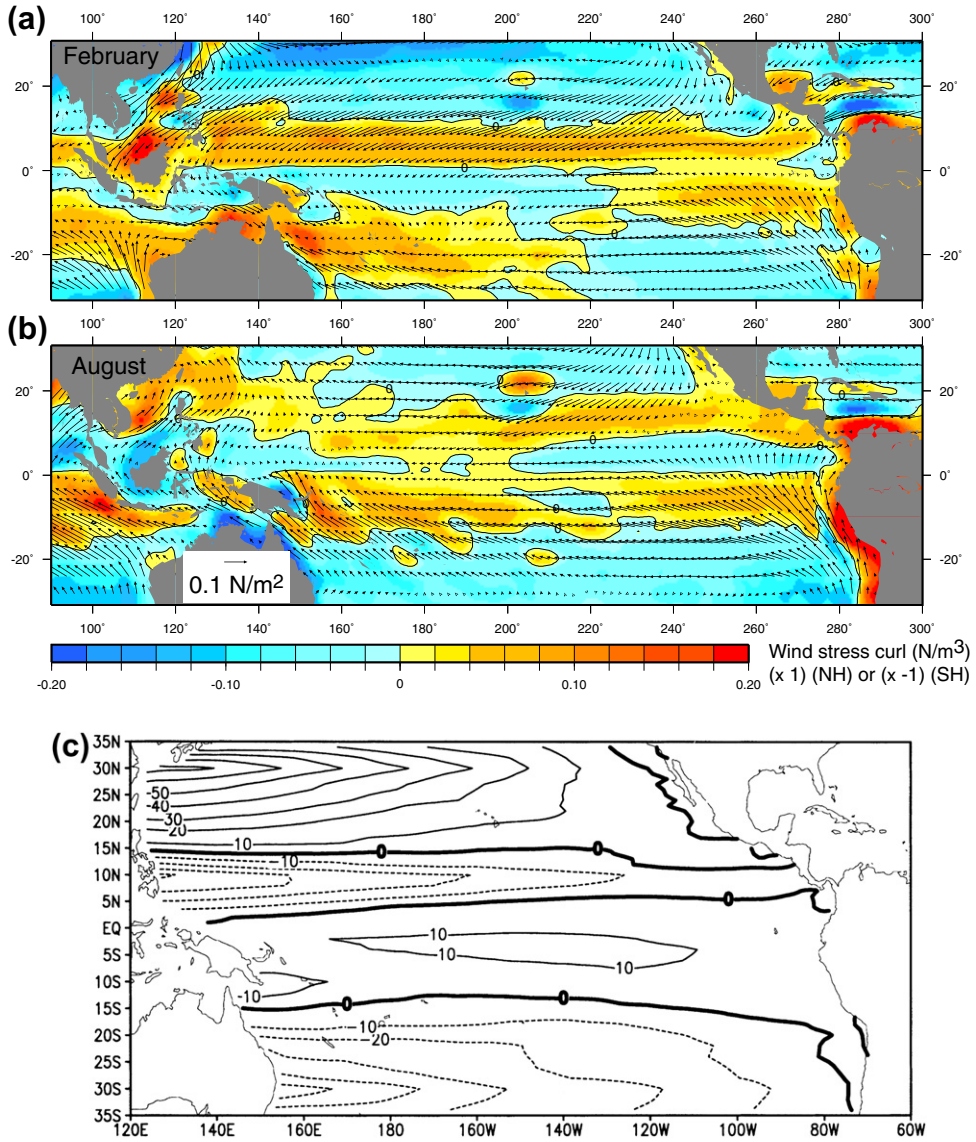

FIGURE S10.16 Climatological wind stress (N/m^2) (vectors) and wind stress curl (N/m^3, multiplied by −1 in Southern Hemisphere; contours, shading is negative): (a) February and (b) August. Monthly mean wind data are from the NCEP reanalysis (Kalnay et al., 1996). (c) Sverdrup transport (Sv) in the tropical Pacific Ocean, calculated from Hellerman-Rosenstein (1983) wind stress. Positive (negative) values yield clockwise (counterclockwise) circulation. ©American Meteorological Society. Reprinted with permission. *Source: From Qu and Lindstrom (2002).*

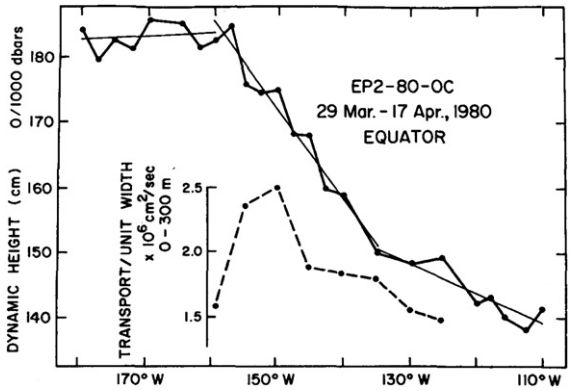

FIGURE S10.17 Dynamic height (dyn cm) along the equator; transport (Sv) of the Equatorial Undercurrent is shown in the inset. ©American Meteorological Society. Reprinted with permission. *Source: From Leetmaa and Spain (1981).*

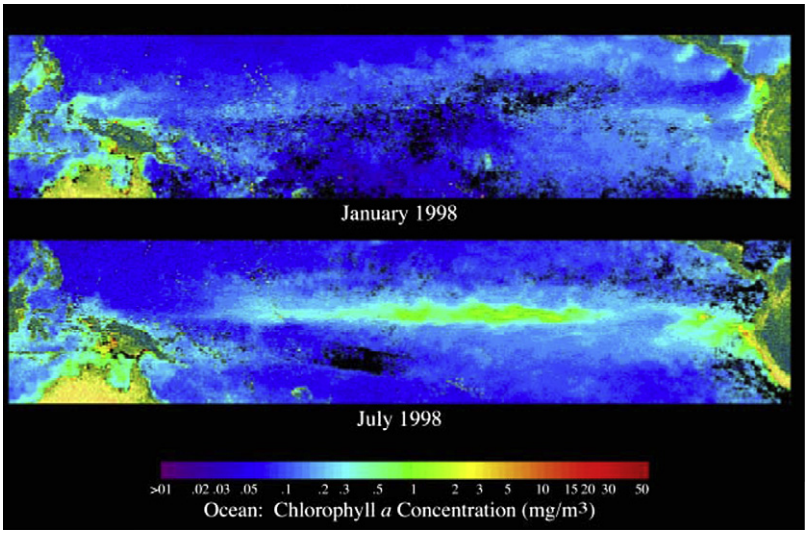

FIGURE S10.18 Chlorophyll composite images from SeaWiFS (January 1998 during El Niño and July 1998 during transition to La Niña). Red = highest chlorophyll contents, dark purple = lowest chlorophyll. *Source: From SeaWiFS Project (2009).*

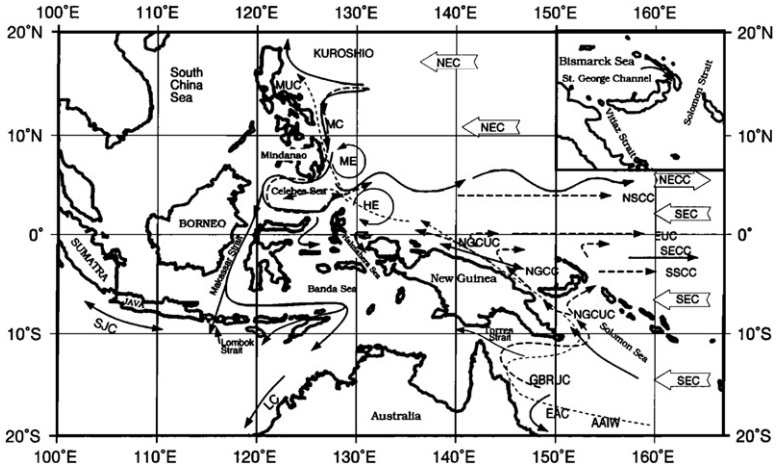

FIGURE S10.19 Currents in the western tropical Pacific. NEC = North Equatorial Current; NECC = North Equatorial Countercurrent; SEC = South Equatorial Current; EUC = Equatorial Undercurrent; NSCC and SSCC = North and South Subsurface Countercurrent; MC = Mindanao Current; MUC = Mindanao Undercurrent; ME = Mindanao Eddy; HE = Halmahera Eddy; NGCC = New Guinea Coastal Current; NGCUC = New Guinea Coastal Undercurrent; GBRUC = Great Barrier Reef Undercurrent; EAC = East Australian Current; LC = Leeuwin Current; AAIW = Antarctic Intermediate Water. *Source: From Lukas, Yamagata, and McCreary (1996); after Fine et al. (1994).*

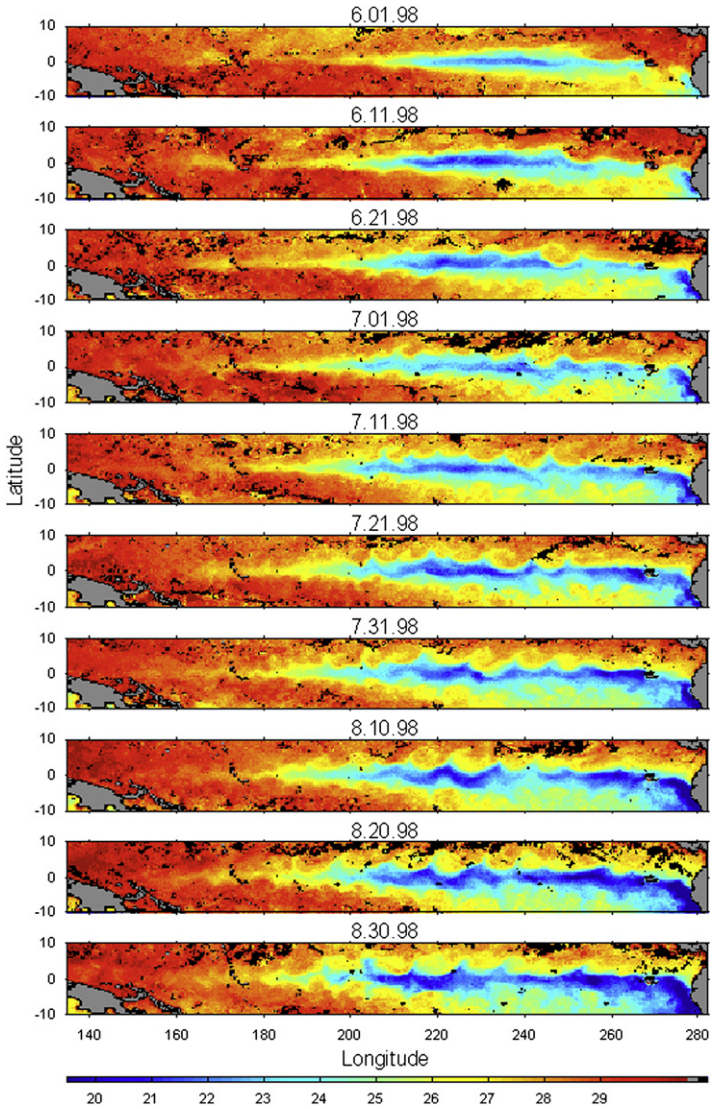

FIGURE S10.20 Tropical sea surface temperature from the Tropical Rainfall Mapping Mission (TRMM) Microwave Imager (TMI) for ten-day intervals from June 1 to August 30, 1998. *Source: From Remote Sensing Systems (2004).*

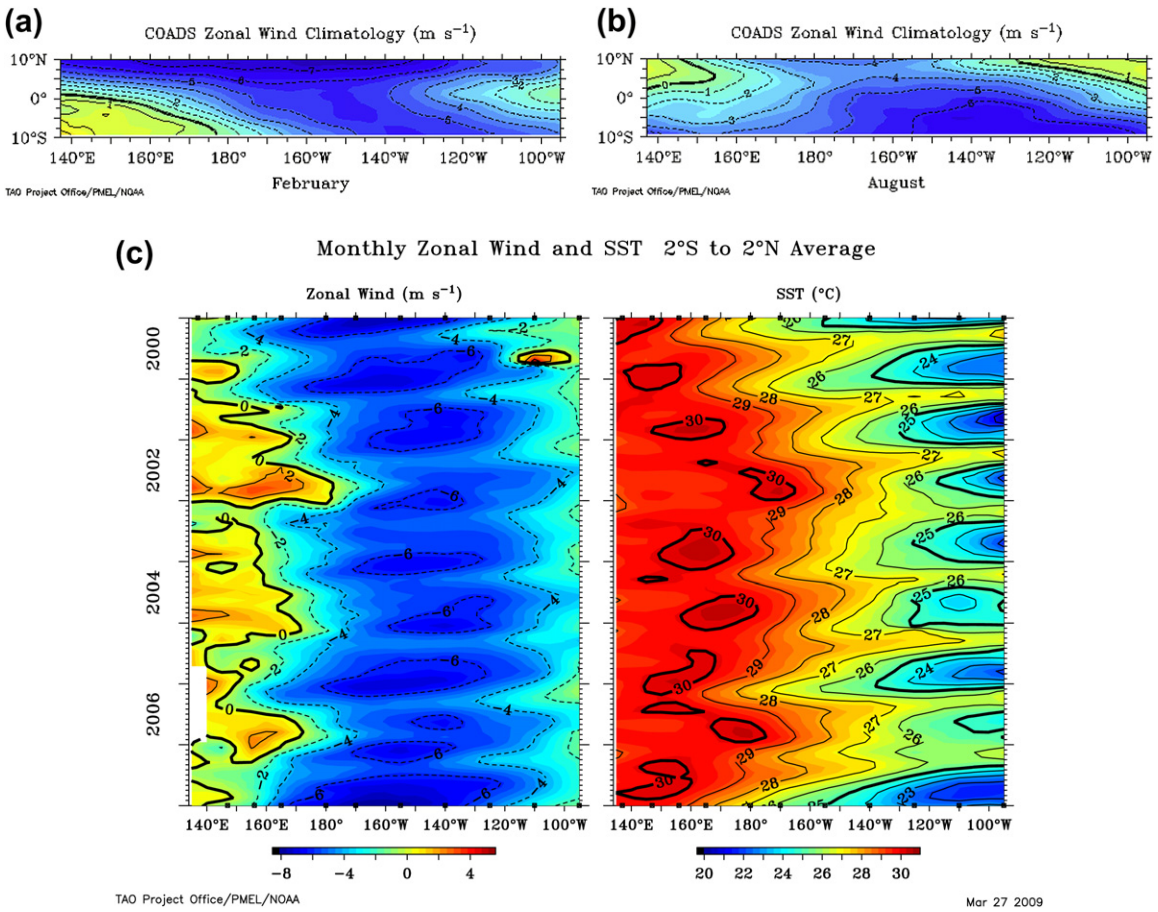

FIGURE S10.21 Winds and SST along the equator in the Pacific. Climatological zonal wind speed in (a) February and (b) August. *Source: From TAO Project Office (2009b).* (c) Monthly zonal wind speed (m/s) and SST (°C). Positive wind is towards the east. *Source: From TAO Project Office (2009a).*

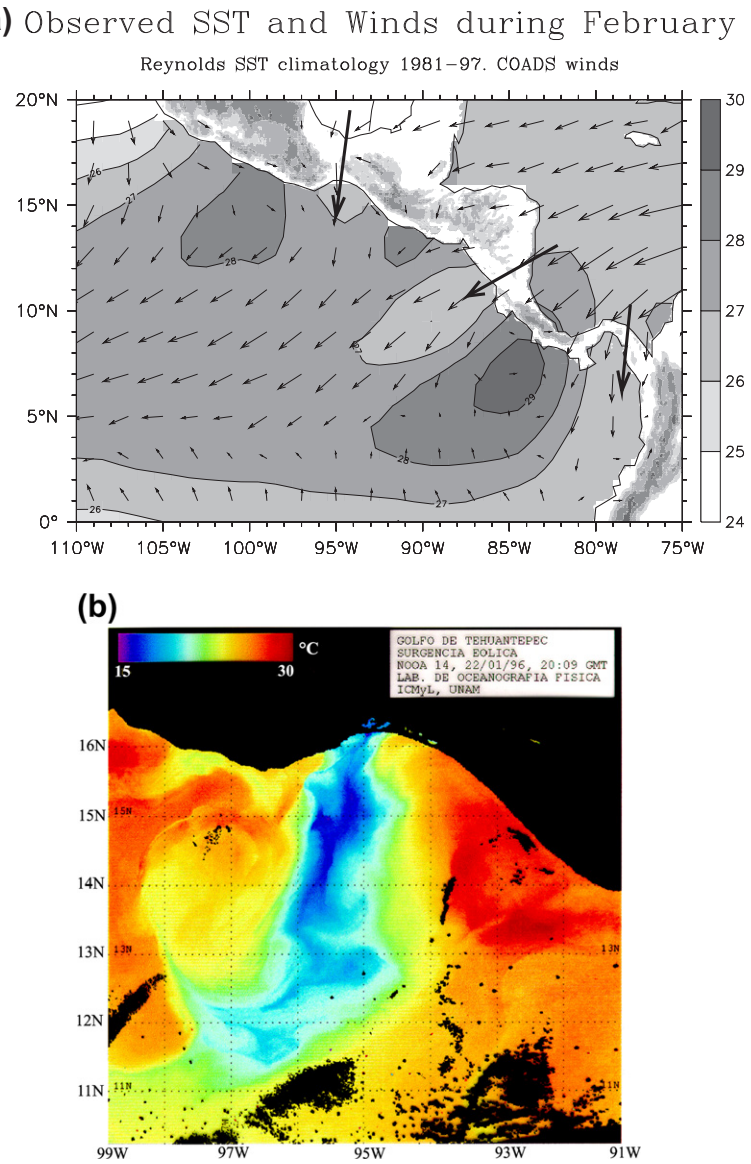

FIGURE S10.22 (a) February mean winds (vectors) from COADS and February mean SST. The large arrows emphasize the gaps through the American cordillera. From north to south: Tehuantepec, Papagayo, and Panama. *Source: From Kessler (2009).* (b) SST in the Gulf of Tehuantepec, January 22, 1996. *Source: From Zamudio et al. (2006).*

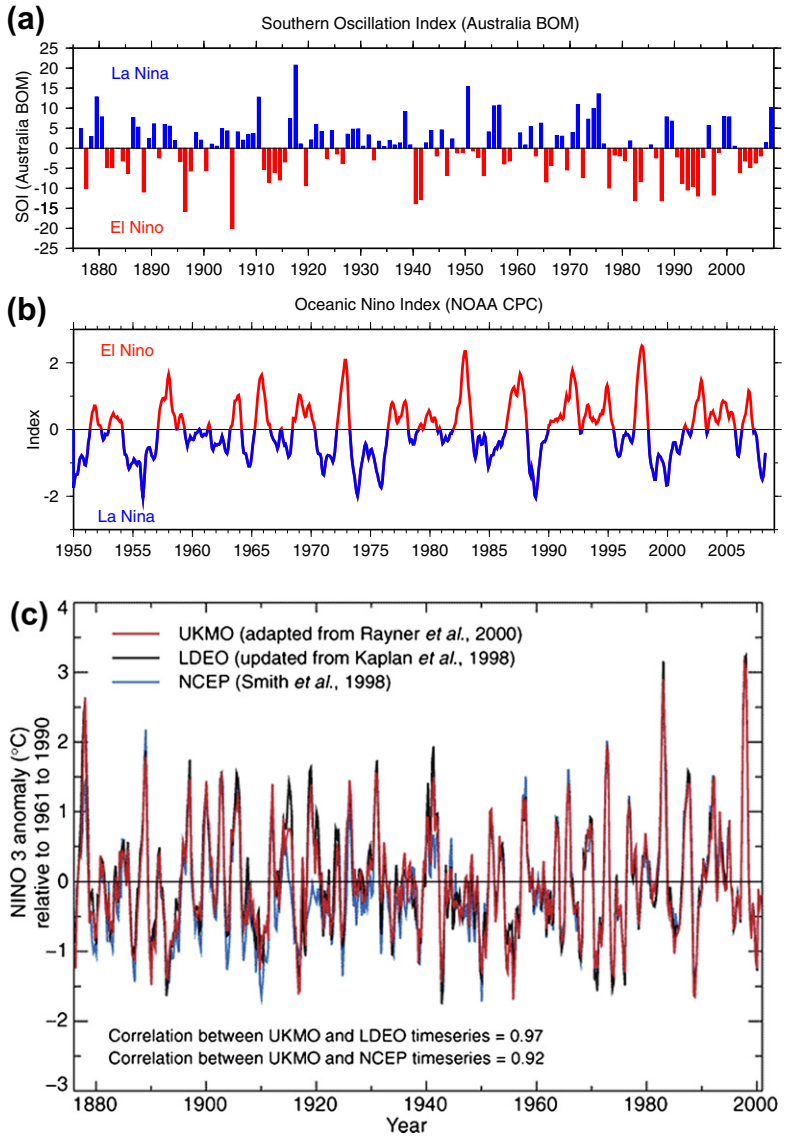

FIGURE S10.23 (a) Southern Oscillation Index (SOI) time series from 1876 to 2008 (annual average). Data from Australian Government Bureau of Meteorology (2009). (b) "Oceanic Nino Index" based on SST in the region 5°N–5°S, 170°W–120°W, as in Figure 10.28b. Red and blue in both panels correspond to El Niño and La Niña, respectively. (c) SST reconstructions from the region 5°N–5°S, 150°W– 90°W. *Source: From IPCC (2001).* (d) Correlation of monthly sea level pressure anomalies with the ENSO Nino3.4 index, averaged from 1948 to 2007. The Nino3.4 index is positive during the El Niño phase, so the signs shown are representative of this phase. *Data and graphical interface from NOAA ESRL (2009b).*

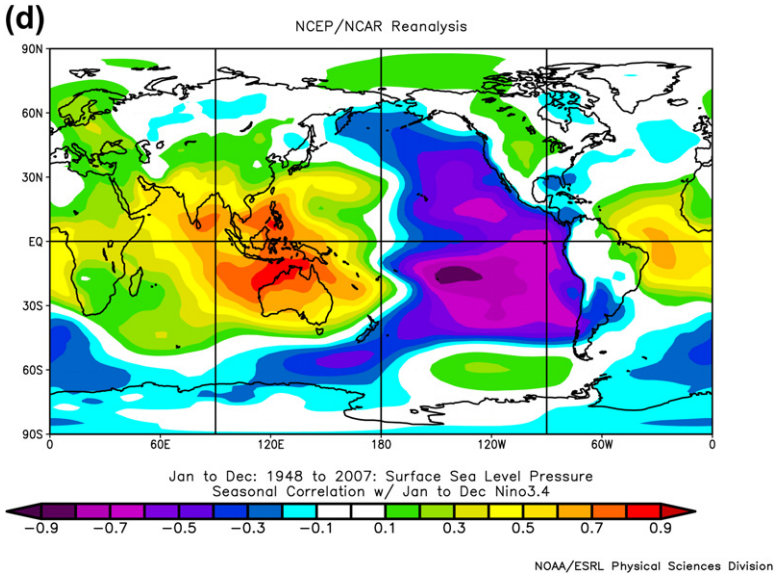

FIGURE S10.23 (*Continued*).

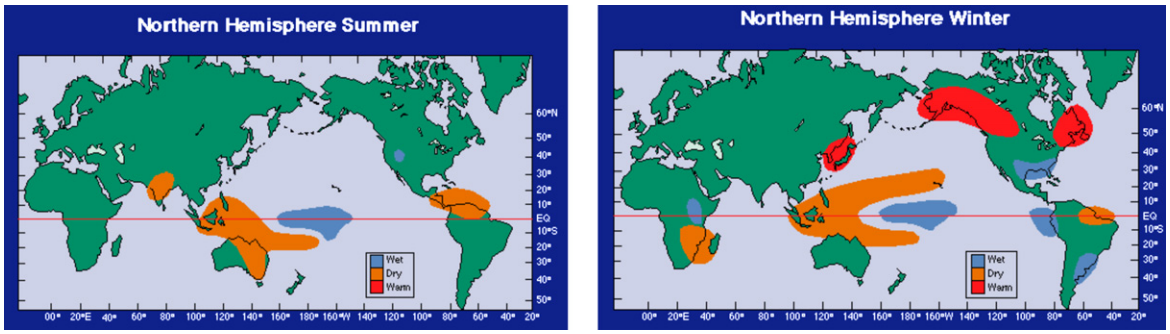

FIGURE S10.24 Global precipitation anomalies for Northern Hemisphere summer (left) and winter (right) during El Niño. *Source: From NOAA PMEL (2009d).*

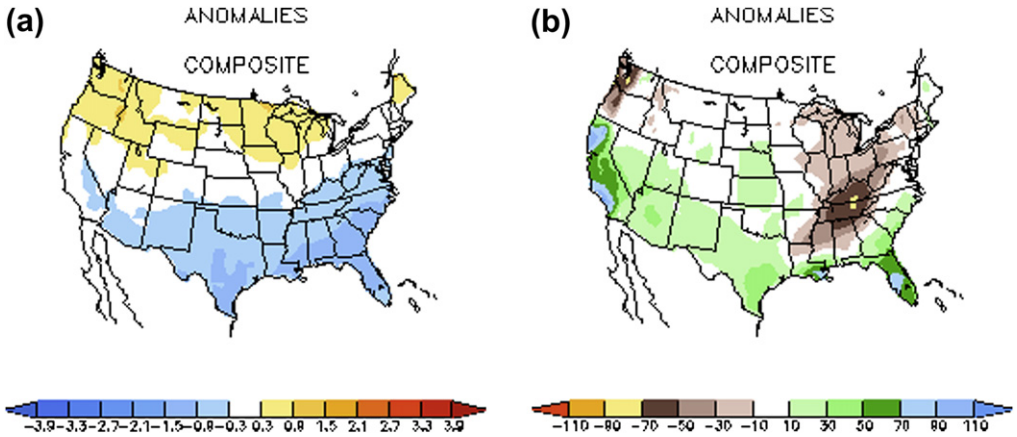

FIGURE S10.25 Anomalies of United States winter (JFM) (a) temperature (°C) and (b) precipitation (mm) during composite El Niño events from 1950 to 2008. *Source: From NWS Internet Services Team (2008).*

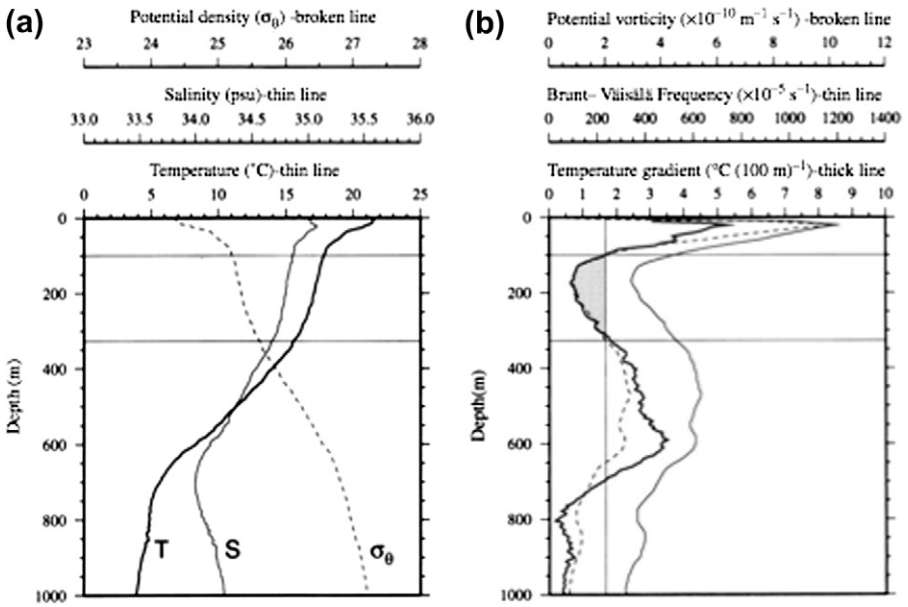

FIGURE S10.26 Subtropical Mode Water. (a) Vertical profile through North Pacific Subtropical Mode Water, at 29° 5′N, 158° 33′E. *Source: From Hanawa and Talley (2001).* (b) North Pacific: thickness of the 17−18 °C layer. *Source: From Masuzawa (1969).* (c) South Pacific: thickness of the 15−17 °C layer. ©American Meteorological Society. Reprinted with permission. *Source: From Roemmich and Cornuelle (1992).*

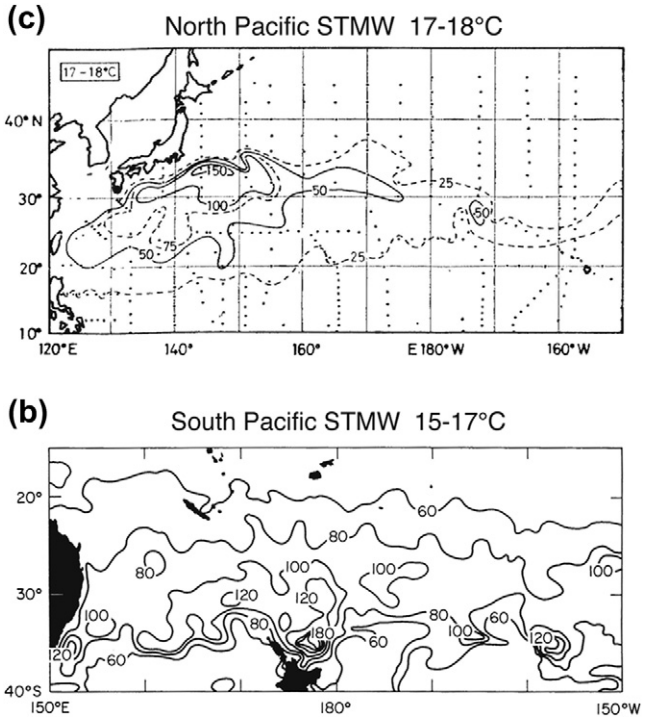

FIGURE S10.26 (*Continued*).

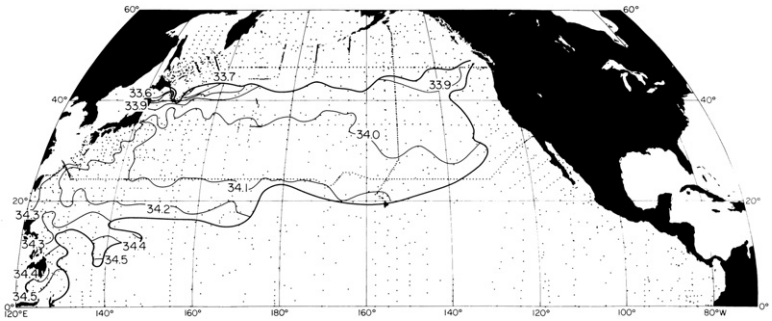

FIGURE S10.27 Salinity at the NPIW salinity minimum. Outer dark contour is the edge of the salinity minimum. ©American Meteorological Society. Reprinted with permission. *Source: From Talley (1993).*

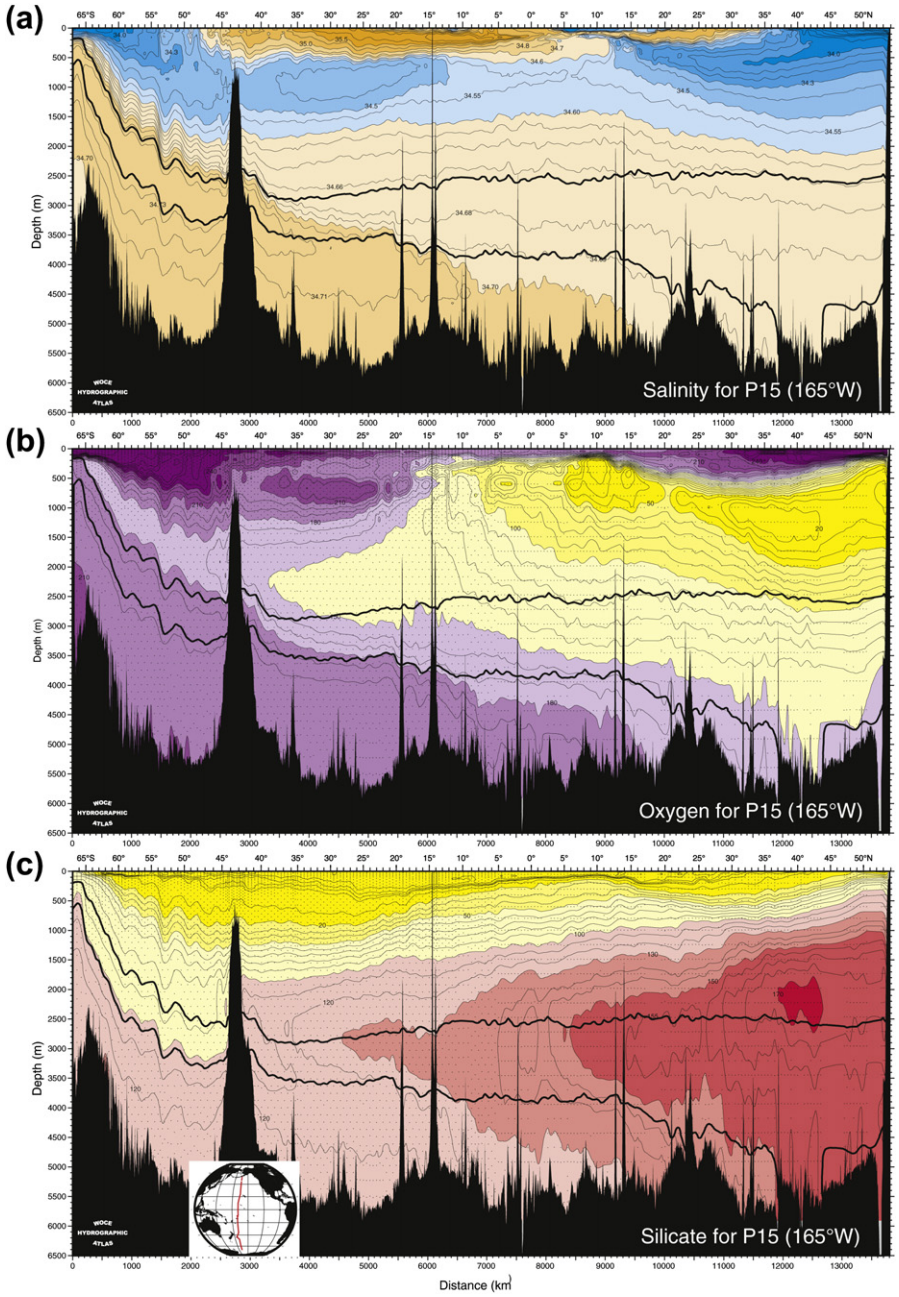

FIGURE S10.28 (a) Salinity, (b) oxygen (μmol/kg), and (c) silicate (μmol/kg) along 165°W. Neutral densities 28.00 and 28.10 kg/m^3 are superimposed. Station locations are shown in inset in (c). *Source: From WOCE Pacific Ocean Atlas, Talley (2007).*

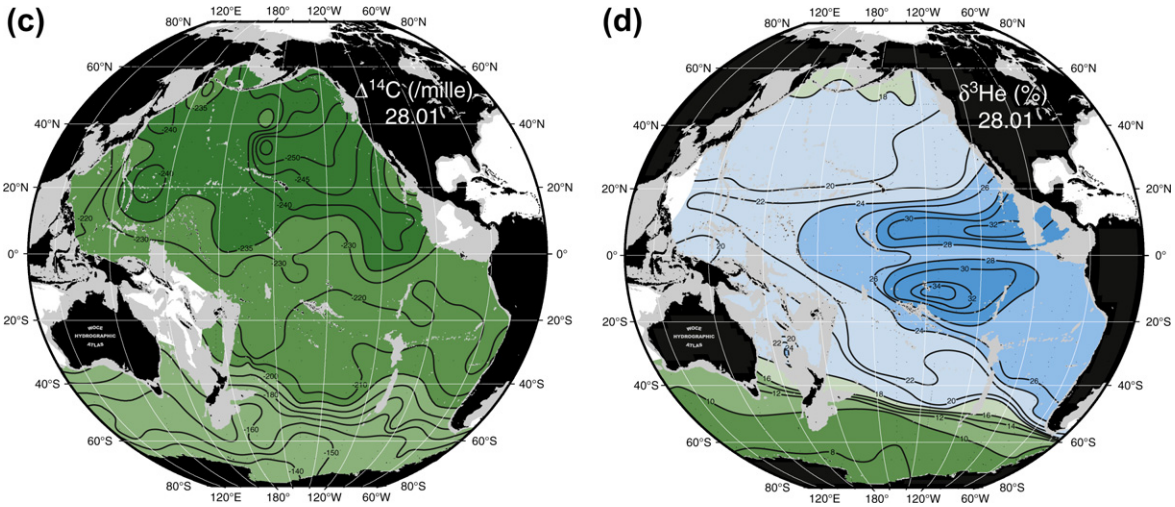

FIGURE S10.29 (a) Salinity, (b) silicate (μmol/kg), (c) $\Delta^{14}C$ (/mille), and (d) $\delta^{3}He$ (%) at neutral density 28.01 kg/m^3 (σ_2 ~ 36.96 kg/m^3), characterizing PDW/UCDW at mid-depth. The depth of the surface is approximately 2600–2800 m north of the Antarctic Circumpolar Current. *Source: From WOCE Pacific Ocean Atlas, Talley (2007).*

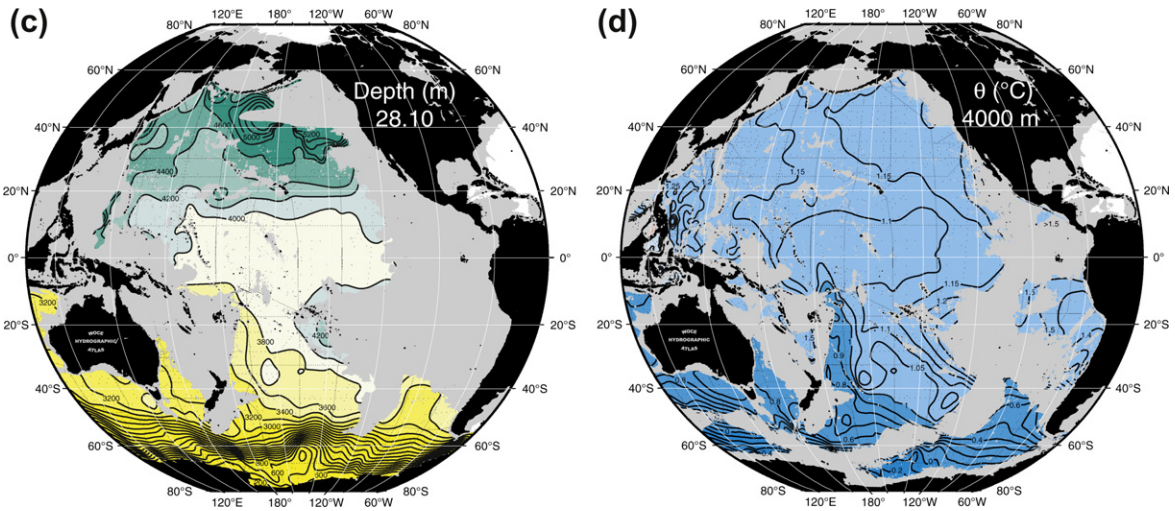

FIGURE S10.30 (a) Salinity, (b) silicate (μmol/kg), and (c) depth (m) at neutral density 28.10 kg/m^3 (σ_4 ~ 45.88 kg/m^3), characteristic of LCDW. (d) Potential temperature at 4000 m. *Source: From WOCE Pacific Ocean Atlas, Talley (2007).*

TABLE S10.1 Major Upper Ocean Circulation Systems, Currents and Fronts of the Mid and High Latitude North Pacific (Figure S10.1)*

Name	Description	Approximate Location
Subtropical gyre	Anticyclonic gyre at mid-latitudes	10–40°N
Subpolar gyre	Cyclonic gyre at mid to high latitudes	40–65°N
Western Subarctic Gyre	Intense cyclonic sub-gyre in the western subpolar gyre	40–55°N, Kuril Islands to 180°
Alaska Gyre	Intense cyclonic sub-gyre in the eastern subpolar gyre	40°N to Alaskan coast, 180° to eastern boundary
Bering Sea gyre	Cyclonic circulation in the Bering Sea	Bering Sea
Okhotsk Sea gyre	Cyclonic circulation in the Okhotsk Sea	Okhotsk Sea
Kuroshio	Subtropical western boundary current	12–35°N
Kuroshio Extension	Subtropical western boundary current extension	35°N
Kuroshio recirculation or Kuroshio Countercurrent	Westward flow just south of the Kuroshio Extension	30°N
Subtropical Countercurrent	Eastward flow of the western subtropical gyre, south of the recirculation; continues into the Subtropical Front	25°N
California Current System	Subtropical eastern boundary current system	23–52°N
Oyashio	Subpolar western boundary current south of central Kuril Islands	40–N
East Kamchatka Current	Subpolar western boundary current north of central Kuril Islands	45–65°N
Alaska Current	Subpolar eastern boundary current	North of 52°N
Alaskan Stream	Southwestward flow of the subpolar gyre along the northern boundary	180–145°W
North Equatorial Current	Westward flow of the subtropical gyre and northern tropical gyre	10–20°N
North Pacific Current	Eastward flow of the subtropical and subpolar gyres	20–50°N
Subtropical Frontal Zone	Zonal frontal band in the subtropical gyre; close to the maximum Ekman transport convergence	30–35°N
Subarctic Frontal Zone	Zonal frontal band separating the subpolar and subtropical gyre regimes; close to maximum westerly wind stress	40–°N

** Shading indicates the basic set.*

TABLE S10.2 South Pacific Circulation Systems and Currents*

Name	Description
Subtropical gyre	Anticyclonic gyre at mid-latitudes
East Australian Current (EAC)	Western boundary current of the subtropical gyre along the coast of Australia
Tasman Front	Eastward current connecting the East Australian Current and the East Auckland Current
East Auckland Current	Western boundary current of the subtropical gyre along the coast of New Zealand
South Pacific Current (or Westwind Drift)	Eastward flow of the subtropical gyre
Subantarctic Front (SAF)	Eastward flow in the northernmost front of the Antarctic Circumpolar Current
Peru-Chile Current System (PCCS)	Eastern boundary current system for the subtropical gyre
Peru-Chile Current (PCC)	Northward flow in the PCCS
Poleward Undercurrent (PUC)	Southward undercurrent in the PCCS
Peru-Chile Countercurrent (PCCC)	Southward surface flow within the PCCS
Cape Horn Current	Southward eastern boundary current
South Equatorial Current	Westward flow of the subtropical gyre

** Shading indicates the basic set.*

TABLE S10.3 Tropical Pacific Currents*

Name	Description	Location Upper Ocean Unless Otherwise Noted
North Equatorial Current (NEC)	Westward flow of the North Pacific subtropical gyre	8–30°N
South Equatorial Current (SEC)	Westward flow of the South Pacific subtropical gyre and westward flow in the equatorial region	30°S to 3°N
North Equatorial Countercurrent (NECC)	Eastward flow between the NEC and SEC	3–8°N
South Equatorial Countercurrent (SECC)	Eastward flow embedded in the SEC	8–11°S, western and central Pacific only
Equatorial Undercurrent (EUC)	Eastward subsurface flow, just below the surface layer	1°S to 1°N 50–250 m
Equatorial Intermediate Current (EIC)	Westward subsurface flow, below the EUC	1°S to 1°N 250–1000 m
Equatorial stacked jets	Reversing subsurface eastward-westward jets, beneath the EIC	1°S to 1°N 1000 m to bottom
North and South Subsurface Countercurrents (NSCC, SSCC; "Tsuchiya jets")	Eastward subsurface flows, off the equator	6–2°S; 2–6°N 150–500 m
Mindanao Current	Southward western boundary current connecting the NEC and NECC	6–14°N
New Guinea Coastal Undercurrent (NGCUC)	Northward tropical western boundary current connecting the SEC and NQC to the EUC, NSCC and SSCC	12°S to 6°N
North Queensland Current (NQC) and Great Barrier Reef Undercurrent (GBRUC)	Northward western boundary current for the SEC	15–12°S (NQC) 23–15°S (GBRUC)

* *Shading indicates the basic set.*

TABLE S10.4 Principal Pacific Ocean Water Masses*

Water Mass	Characteristic in the Vertical	Layer	Process
North Pacific Central Water (NPCW)	Subtropical thermocline waters	Upper 0–1000 m	Subduction
South Pacific Central Water (SPCW)	Subtropical thermocline waters	Upper 0–1000 m	Subduction
North Pacific Subtropical Underwater (NPSTUW)	Subtropical/tropical salinity maximum	Upper 100–200 m	Subduction of high salinity subtropical surface waters
South Pacific Subtropical Underwater (SPSTUW)	Subtropical/tropical salinity maximum	Upper 100–200 m	Subduction of high salinity subtropical surface waters
North Pacific Subtropical Mode Water (NPSTMW)	Subtropical stability (potential vorticity) minimum	Upper 0–400 m	Subduction of thick winter mixed layer
South Pacific Subtropical Mode Water (SPSTMW)	Subtropical stability (potential vorticity) minimum	Upper 0–300 m	Subduction of thick winter mixed layer
Subantarctic Mode Water (SAMW)	Southern subtropical stability (potential vorticity) minimum	Upper 0–600 m	Subduction of thick winter mixed layer from Subantarctic Front
Dichothermal Water (DtW)	North Pacific subpolar temperature minimum	Upper 0–150 m	Advection of cold subpolar surface waters
Mesothermal Water (MtW)	North Pacific subpolar temperature maximum	Upper 200–500 m	Advection of warmer near-surface subpolar waters
North Pacific Intermediate Water (NPIW)	Salinity minimum in subtropical North Pacific	Intermediate 200–800 m	Advection of fresh subpolar surface water
Antarctic Intermediate Water (AAIW)	Salinity minimum in subtropical North Pacific and tropical Pacific	Intermediate 500–1200 m	Advection of fresh subantarctic surface water
Pacific Deep Water (PDW)	Oxygen minimum, nutrient maximum	Deep 1000–4000 m	Mixing and aging of deep waters
Upper Circumpolar Deep Water (UCDW)	High oxygen, low nutrients, high salinity on isopycnal surfaces	Deep ~ 1000–3000 m	Mixture of deep waters in the Southern Ocean
Lower Circumpolar Deep Water (LCDW)	Deep salinity and oxygen maxima, nutrient minima	Bottom 3000 m to bottom	Brine rejection in the Southern Ocean mixed with NADW, PDW, and IDW

* *Shading indicates the basic set.*

References

Australian Government Bureau of Meteorology, 2009. S.O.I (Southern Oscillation Index) Archives — 1876 to present. http://reg.bom.gov.au/climate/current/soihtm1.shtml (accessed 03.27.09).

Crawford, W., 2002. Physical characteristics of Haida Eddies. J. Oceanogr 58, 703–713.

Davis, R.E., 2005. Intermediate-depth circulation of the Indian and South Pacific Oceans measured by autonomous floats. J. Phys. Oceanogr 35, 683–707.

Favorite, F., Dodimead, A.J., Nasu, K., 1976. Oceanography of the subarctic Pacific region, 1960–71. International North Pacific Fisheries Commission, ew, 33, 187 pp.

Fine, R.A., Lukas, R., Bingham, F.M., Warner, M.J., Gammon, R.H., 1994. The western equatorial Pacific: A water mass crossroads. J. Geophys. Res. 99, 25063–25080.

Ganachaud, A., 2003. Large-scale mass transports, water mass formation, and diffusivities estimated from World Ocean Circulation Experiment (WOCE) hydrographic data. J. Geophys. Res. 108 (C7), 3213. doi: 10.1029/2002JC002565.

Hanawa, K., Talley, L.D., 2001. Mode Waters. In: Siedler, G., Church, J. (Eds.), Ocean Circulation and Climate. International Geophysics Series. Academic Press, pp. 373–386.

IPCC, 2001. Climate Change 2001: The Scientific Basis. In: Houghton, J.T., Ding, Y., Griggs, D.J., Noguer, M., van der Linden, P.J., Dai, X., Maskell, K., Johnson, C.A. (Eds.), Contribution of Working Group I to the Third Assessment Report of the Intergovernmental Panel on Climate change. Cambridge University Press, Cambridge, UK and New York, 881 pp.

Kalnay, E., Kanamitsu, M., Kistler, R., Collins, W., Deaven, D., Gandin, L., 1996. The NCEP-NCAR 40-year reanalysis project. B. Am. Meteorol. Soc. 77, 437–471.

Kawabe, M., Yanagimoto, D., Kitagawa, S., 2006. Variations of deep western boundary currents in the Melanesian Basin in the western North Pacific. Deep-Sea Res. I 53, 942–959.

Kessler, W.S., 2009. The Central American mountain-gap winds and their effects on the ocean. http://faculty.washington.edu/kessler/t-peckers/t-peckers.html (accessed 3.27.09).

Kono, T., Kawasaki, Y., 1997. Modification of the western subarctic water by exchange with the Okhotsk Sea. Deep-Sea Res. I 44, 689–711.

Leetmaa, A., Spain, P.F., 1981. Results from a velocity transect along the equator from 125 to 159°W. J. Phys. Oceanogr. 11, 1030–1033.

Lukas, R., Yamagata, T., McCreary, J.P., 1996. Pacific low-latitude western boundary currents and the Indonesian throughflow. J. Geophys. Res. 101, 12209–12216.

Mackas, D.L., Strub, P.T., Thomas, A., Montecino, V., 2006. Eastern ocean boundaries pan-regional overview. In: Robinson, A.R., Brink, K.H. (Eds.), The Sea, Vol. 14A: The Global Coastal Ocean: Interdisciplinary Regional Studies and Syntheses. Harvard University Press, pp. 21–60.

Masuzawa, J., 1969. Subtropical Mode Water. Deep-Sea Res. 16, 453–472.

Mata, M.M., Wijffels, S.E., Church, J.A., Tomczak, M., 2006. Eddy shedding and energy conversions in the East Australian Current. J. Geophys. Res. 111, C09034. doi:10.1029/2006JC003592.

McClain, C., Christian, J.R., Signorini, S.R., Lewis, M.R., Asanuma, I., Turk, D., Dupouy-Douchement, C., 2002. Satellite ocean-color observations of the tropical Pacific Ocean. Deep-Sea Res. II 49, 2533–2560.

NASA Visible Earth, 2008. Eddies off the Queen Charlotte Islands. NASA Goddard Space Flight Center. http://visibleearth.nasa.gov/view_rec.php?id=2886 (accessed 3.26.09).

Niiler, P.P., Maximenko, N.A., McWilliams, J.C., 2003. Dynamically balanced absolute sea level of the global ocean derived from near-surface velocity observations. Geophys. Res. Lett. 30, 22. doi:10.1029/2003GL018628.

NOAA ESRL, 2009b. Linear correlations in atmospheric seasonal/monthly averages. NOAA Earth System Research Laboratory Physical Sciences Division. http://www.cdc.noaa.gov/data/correlation/ (accessed 10.30.09).

NOAA PMEL, 2009d. Impacts of El Niño and benefits of El Niño prediction. NOAA Pacific Marine Environmental Laboratory. http://www.pmel.noaa.gov/tao/elnino/impacts.html (accessed 3.26.09).

NWS Internet Services Team, 2008. ENSO temperature and precipitation composites. http://www.cpc.noaa.gov/products/precip/CWlink/ENSO/composites/EC_LNP_index.shtml (accessed 3.27.09).

Qiu, B., Scott, R.B., Chen, S., 2008. Length scales of eddy generation and nonlinear evolution of the seasonally modulated South Pacific Subtropical Countercurrent. J. Phys. Oceanogr. 38, 1515–1528.

Qu, T., Lindstrom, E., 2002. A climatological interpretation of the circulation in the western South Pacific. J. Phys. Oceanogr. 32, 2492–2508.

Remote Sensing Systems, 2004. TMI sea surface temperatures (SST). http://www.ssmi.com/rss_research/tmi_sst_pacific_equatorial_current.html (accessed 3.27.09).

Ridgway, K.R., Dunn, J.R., 2003. Mesoscale structure of the mean East Australian Current System and its relationship with topography. Progr. Oceanogr. 56, 189–222.

Roden, G.I., 1991. Subarctic-subtropical transition zone of the North Pacific: Large-scale aspects and mesoscale structure. In: Wetherall, J.A. (Ed.), Biology, Oceanography and Fisheries of the North Pacific Transition Zone

and the Subarctic Frontal Zone. NOAA Technical Report 105, 1–38.

Roemmich, D., Cornuelle, B., 1992. The Subtropical Mode Waters of the South Pacific Ocean. J. Phys. Oceanogr. 22, 1178–1187.

SeaWiFS Project, 2009. SeaWiFS captures El Nino-La Nina transitions in the equatorial Pacific. NASA Goddard Space Flight Center. http://oceancolor.gsfc.nasa.gov/SeaWiFS/BACKGROUND/Gallery/pac_elnino.jpg (accessed 3.26.09).

Sekine, Y., 1999. Anomalous southward intrusions of the Oyashio east of Japan 2. Two-layer numerical model. J. Geophys. Res. 104, 3049–3058.

Talley, L.D., 1993. Distribution and formation of North Pacific Intermediate Water. J. Phys. Oceanogr 23, 517–537.

Talley, L.D., 2007. Hydrographic Atlas of the World Ocean Circulation Experiment (WOCE). In: Sparrow, M., Chapman, P., Gould, J. (Eds.), Pacific Ocean, Volume 2. International WOCE Project Office, Southampton, U.K. ISBN 0-904175-54-5.

TAO Project Office, 2009a. TAO/TRITON data display and delivery. NOAA Pacific Marine Environmental Laboratory. http://www.pmel.noaa.gov/tao/disdel/disdel.html (accessed 3.27.09).

TAO Project Office, 2009b. TAO Climatologies. NOAA Pacific Marine Environmental Laboratory. http://www.pmel.noaa.gov/tao/clim/clim.html (accessed 7.5.09).

Zamudio, L., Hurlburt, H.E., Metzger, E.J., Morey, S.L., O'Brien, J.J., Tilburg, C.E., Zavala-Hidalgo, J., 2006. Interannual variability of Tehuantepec eddies. J. Geophys. Res. 111, C05001. doi:10.1029/2005JC003182.